ORGANOMETALLICS

Article

pubs.acs.org/Organometallics

Synthetic and Spectroscopic Study of the Mechanism of Atomic Layer Deposition of Tin Dioxide

Matthew S. Weimer,[†] Bo Hu,[†,∥] Steven J. Kraft,[∥] Roy G. Gordon,[⊥] Carlo U. Segre,[‡,§] and Adam S. Hock*[,†,§,∥]

[†]Department of Chemistry, [‡]Department of Physics, and [§]Center for Synchrotron Radiation Research and Instrumentation, Illinois Institute of Technology, 3101 South Dearborn Street, Chicago, Illinois 60616, United States

[⊥]Department of Chemistry and Chemical Biology, Harvard University, 12 Oxford Street, Cambridge, Massachusetts 02138, United States

[∥]Chemical Sciences and Engineering Division, Argonne National Laboratory, 9700 South Cass Avenue, Argonne, Illinois 60439, United States

Supporting Information

ABSTRACT: This study details the surface reaction chemistry relevant to the vapor deposition mechanism of SnO_2 thin films by atomic layer deposition. The mechanism was elucidated by combining different spectroscopic studies. Initial nucleation of cyclic N^2,N^3-di-*tert*-butylbutane-2,3-diamidotin(II) (**1**) consists of surface SiOH protonation of ligands as shown by diffuse reflectance infrared Fourier transform spectroscopy (DRIFTS). This SiO_2-surface-bound stannylene was further characterized by X-ray absorption (XAS) and resonance Raman spectroscopy. XAS, DRIFTS, and Raman spectroscopy were then used to follow the further reaction of the surface-bound stannylene with different oxygen sources and a second equivalent of **1**. It was observed that water does not oxidize the initial surface-bound tin site, and a well-defined, three-coordinate tin(II) species, with two surface oxygen bonds and one coordinated water molecule, was characterized. Treatment of the surface stannylene with protic oxidants such as H_2O_2 or *t*BuOOH fully oxidizes tin to 4+, and coordination of additional oxygen ligands is observed. When a second equivalent of **1** is added to surface-bound Sn^{4+}, the resulting surface tin is also found to be in the 4+ oxidation state, contrary to the nonoxidative nucleation step. As such, surface peroxide species provide a probable growth mechanism of SnO_2 through oxidation, while nucleation occurs through protic ligand exchange.

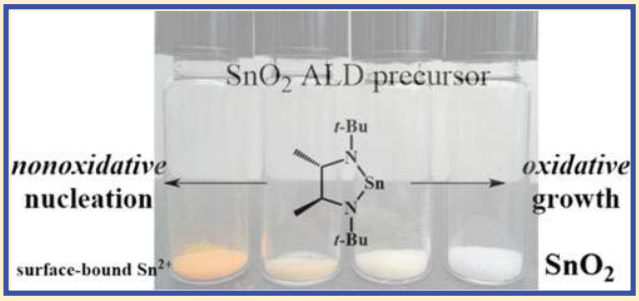

INTRODUCTION

The controlled synthesis of well-defined materials for catalytic[1] and electronic[2] applications is dependent on intimate knowledge of chemical processes. This is particularly challenging for gas−solid reactions, such as in the rapidly growing field of atomic layer deposition (ALD), where sequential, stoichiometric reactions of gaseous metal and nonmetal sources are used to grow a material. By far the most common strategy for deposition relies on proton transfer followed by ligand dissociation as the synthetic pathway, e.g., oxides, sulfides, and nitrides prepared from metal precursor and corresponding protic reagents H_2O, H_2S, and H_3N.[3] In addition to water, other oxygen sources such as molecular oxygen, ozone, and hydrogen peroxide have been used to prepare metal oxide films. In general, little attention has been paid to the role that the nonmetal "precursor" (reagent) plays in the chemistry beyond whether it is acting as a proton-containing reagent or an oxidant. However, utilizing more complicated chemistry for ALD processes requires a detailed understanding of the impact of metal and nonmetal reagents upon both nucleation and growth mechanisms.

One new synthetic strategy for growth by ALD is controlled oxidation of a lower valent metal starting material. This is advantageous because the nature of the oxidant can control the oxidation state and structure of the resulting metal oxide species, as has been shown in the case of iron oxides.[4] Furthermore, lower valent complexes require fewer ligands and therefore *can* be more volatile, which has been demonstrated by our group for iron[4] and tin oxides.[5] In the case of tin, a low-valent tin(II) precursor (Figure 1) has been shown to be quite versatile for the synthesis of tin chalcogenides. This tin(II) compound (**1**) can be used with H_2S as an ALD partner to grow the photovoltaic material SnS by a protonation ALD mechanism.[6] Also, **1** can be used with H_2O_2 to grow SnO_2 by an oxidation mechanism. Interestingly, SnO does not grow when H_2O is used as an ALD partner.[5]

Received: December 14, 2015
Published: April 18, 2016

DOI: 10.1021/acs.organomet.5b01004
Organometallics 2016, 35, 1202−1208

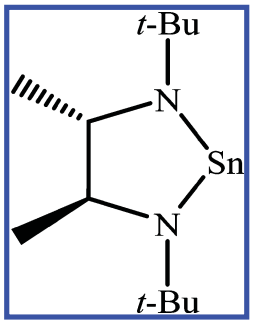

Figure 1. Stannylene, N_2,N_3-di-*tert*-butylbutane-2,3-diamidotin(II) (**1**), previously reported to be an ALD precursor for growth of SnS with H_2S and SnO_2 with H_2O_2.

Since stannylenes show reactivity through oxidation as well as ligand exchange, mechanisms for ALD growth are not simple to predict. Issues arise from the ability to anticipate whether a stannylene will react through oxidative addition versus protolytic ligand transfer, as outlined in Scheme 1. Intuitively,

Scheme 1. Potential Pathways for a Low-Valent Stannylene Compound with Protic Species: Path A Is a Protonation Reaction, Path B Is Lewis Acid/Base Coordination, and Path C Is Oxidative Addition

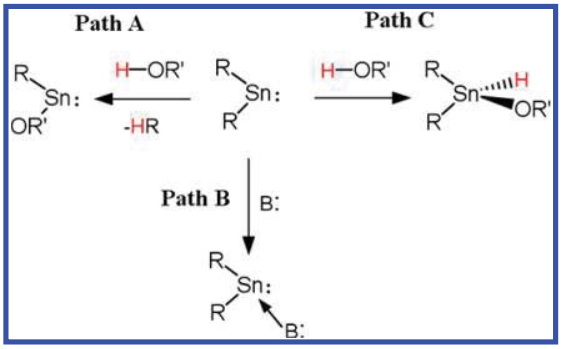

it is anticipated that a more acidic proton would induce protolytic ligand transfer and a more basic compound could induce oxidative addition. However, Power and co-workers have established that reactivity of diarylstannylenes depends less on the pK_a of the reagent or the steric bulk of the arene groups than the thermodynamic stability of the products and kinetics of the reaction. For instance, the bulky stannylene $Sn(Ar^{Me6})_2$, [Ar^{Me6} = C_6H_3-2,6-(C_6H_2-2,4,6-$(CH_3)_3)_2$] undergoes arene elimination with H_2 and NH_3 (pK_a = 10.5) to remain 2+[7] and oxidative addition with HBF_4 (pK_a = −0.44) and $H(SO_3CF_3)$ (pK_a = −14.1) to form Sn(IV) compounds.[8] Complicating the matter further, stannylenes have shown a wide range of additional reactivity: coordination via the lone pair to transition metals[9] or as Lewis acid–base pairs with carbenes,[10] insertion,[11] reduction (disproportionation to Sn metal), cycloaddition,[12] and substitution[13] reactions.

ALD of SnO_2 films has been successful using a wide range of precursors;[3] however recent use of stannylenes has been found to grow films with superior quality and electrical properties.[5,14] Clean, stoichiometric reactivity is absolutely necessary for ALD of quality materials, most prominently at interfaces. The stoichiometric nature of an ALD reaction, where a maximum of one monolayer of precursor can react with the active surface species during each half-cycle, allows for the growth mechanism, in theory, to be studied with traditional solution chemistry.[15] Thus, the chemistry of **1** provides an ideal setting to study the solution and surface coordination chemistry of stannylenes with oxidants and hydroxide (−OH) bonds. We wish to report the discovery of the deposition mechanism reaction of a cyclic stannylene with H_2O_2.

RESULTS AND DISCUSSION

While the successful deposition of SnO_2 from N^2,N^3-di-*tert*-butylbutane-2,3-diamidotin(II) (**1**) and H_2O_2 has been performed for years,[5] the mechanism, specifically how and when tin is oxidized, has not yet been studied in detail. Generally, stannylenes have access to different reaction paths, as shown in Scheme 1, depending on the geometry and availability of the tin p-type orbitals. Low-coordinate heterocyclic stannylenes show similar reactivity to the general class of stannylene mentioned above; however, **1** does not have the stability of additional nitrogen π-donors to mitigate the reactivity of the unfilled p-orbital. As such, coordinately unsaturated compounds similar to **1** are expected to undergo more facile oxidative addition compared to ligand transfer/protonation or acid/base donor chemistry. Foley et al. showed facile protonation chemistry of bis(dimethylamido)tin(II) with ethanol to give $Sn(OR)_2$,[16] and Tolman and co-workers showed the conversion and isolation of a bis(amidinate)tin(II) compound to the monosubstituted tin(II) alcohol was aided by the steric bulk of the reactants.[13b] Additionally, Neumann remarks how dialkyl stannylenes are expected to make Lewis acid–base donor pairs with small Lewis bases, such as H_2O;[17] unfortunately the authors are not aware of any single-molecule examples of this type of Lewis acid–base compound to date. Recently, Power and co-workers found that diarlygermylenes and diarylstannylenes exhibit oxidative addition behavior with Brønsted acids. For example, Ar_2Sn oxidizes to Sn(IV) with HBF_4.[8] These works outline three distinct pathways for reaction with protic oxygen sources, as shown in Scheme 1; substitution through protonation, coordination of a Lewis base to the empty p-orbital of the Sn, and oxidative addition to generate a Sn(IV) species.

Access to the different mechanisms of stannylene reactivity is observed in ALD literature, as these types of coordinately unsaturated precursors will grow SnS[14c] with H_2S and SnO_2 with H_2O_2.[5] Interestingly, these cyclic stannylenes do not appreciably grow SnO with H_2O under ALD conditions. This disparate behavior is worthy of further investigation. In solution, **1** reacts with H_2O and H_2O_2 to form an insoluble solid. Further investigative reactions with triphenylsilanol gave a mixture of products that were difficult to characterize by ^{1}H NMR and, in our hands, did not produce an isolable product.

To overcome the difficulty faced in solution with **1**, we produced a material that contains isolated stannylene species on dehydrated high-surface-area silica (SiO_2). Synthesis of **1** with SiO_2 proceeded quickly in organic solvents at room temperature, where an orange solution of **1** reacts with white SiO_2 to give light orange **2**, as shown in Figure 2b–d. The clear mother liquor was devoid of starting material by ^{1}H NMR at this point, and heating **2** in benzene-d_6 to 60 °C for 30 min showed just under an equivalent of free ligand in solution, compared to an internal standard, and was observed across molar loading on the SiO_2 surface. Molar loading was kept at 1.5 mol % for all further investigations. Loss of ligand around the Sn center in material **2** is further supported by X-ray absorption near edge structure (XANES) spectroscopy; the

DOI: 10.1021/acs.organomet.5b01004
Organometallics 2016, 35, 1202–1208

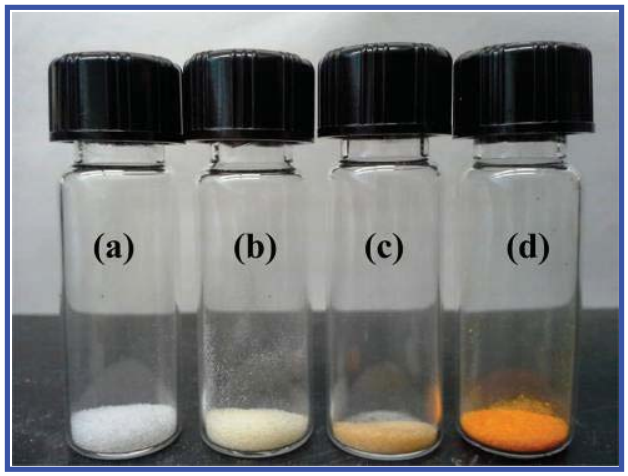

Figure 2. N^2,N^3-Di-*tert*-butylbutane-2,3-diamidotin(II) (**1**) molar loading levels of (a) 0 mol %, (b) 1.5 mol %, (c) 3.0 mol %, and (d) 4.5 mol % on SiO_2.

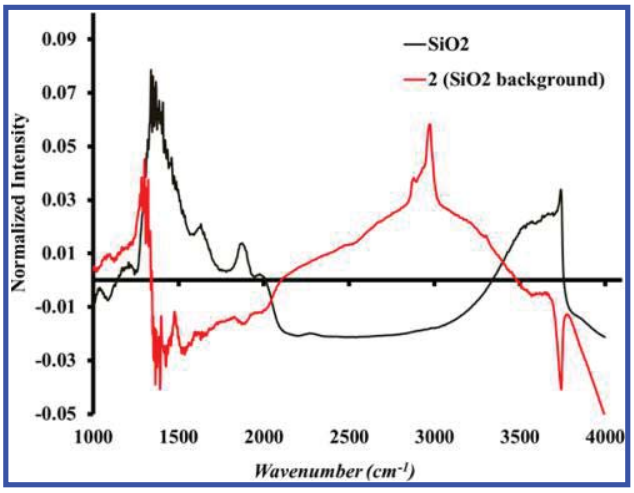

Figure 4. Diffuse reflectance infrared Fourier transform spectroscopy (DRIFTS) of unreacted silica (black) and the product of **1** with silica (**2**) with SiO_2 as a background shown in red.

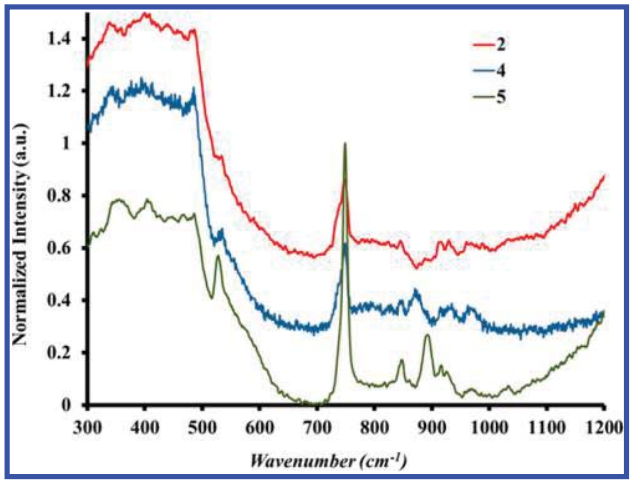

Figure 5. Raman spectra of materials **2**, **4**, and **5** that were taken directly after the conclusion of each reaction. Spectra are offset for clarity.

excitation energy for the 1s electron or edge position is the same for the SnO standard (tabulated in the Supporting Information, Table S1), but the shape is drastically different from **1**, as shown in Figure 3. The change in shape is due to the difference in orbital contribution to the LUMO on Sn between two $^{-}NR_2$ ligands and two $^{-}OSi^*$ ($^{-}OSi^*$ indicates a surface species) ligands. Ligand exchange is also confirmed with diffuse reflectance infrared Fourier transform spectroscopy (DRIFTS). Material **2** shows a decrease in the band associated with the surface hydroxyl of high surface area silica (3743 cm^{-1})[18] after addition of the Sn(II) precursor (**1**), as shown in the SiO_2 background-subtracted spectrum in Figure 4. Additionally, the spectra show the existence of a protonated ligand on the surface of the SiO_2, where the NH stretch was observed at 3310 cm^{-1}, close to the published value of 3307 cm^{-1}.[19] No nitrogen was observed in the films grown by Gordon and co-workers,[5] and the NMR data showed release of a full equivalent of protonated ligand; it is assumed that free ligand does not interfere with the surface growth chemistry and is removed during growth conditions. To ensure isolated Sn species, we maintained a low molar loading, 0.015 mol (1.5 mol %), of Sn/mol of surface hydroxyls (Figure 2b). The single-site nature of **2** is confirmed by Raman spectroscopy, shown in Figure 5, through the absence of a peak at 580 cm^{-1} associated with SnO_2 clusters[20] and X-ray absorption fine structure (XAFS), where approx-

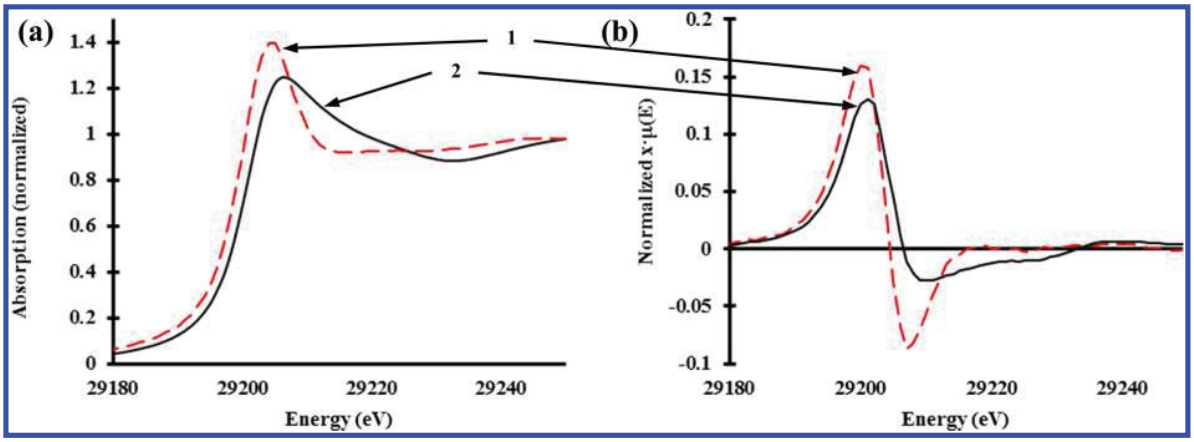

Figure 3. (a) XANES spectra of N^2,N^3-di-*tert*-butylbutane-2,3-diamidotin(II) (**1**) with as-deposited **2** and (b) the first derivative of the same XAS data.

DOI: 10.1021/acs.organomet.5b01004
Organometallics 2016, 35, 1202−1208

Scheme 2. Reaction Pathways for 2 with Various Oxygen Sources as Well as a Second Molar Equivalent of N^2,N^3-Di-*tert*-butylbutane-2,3-diamidotin(II) (1)[a]

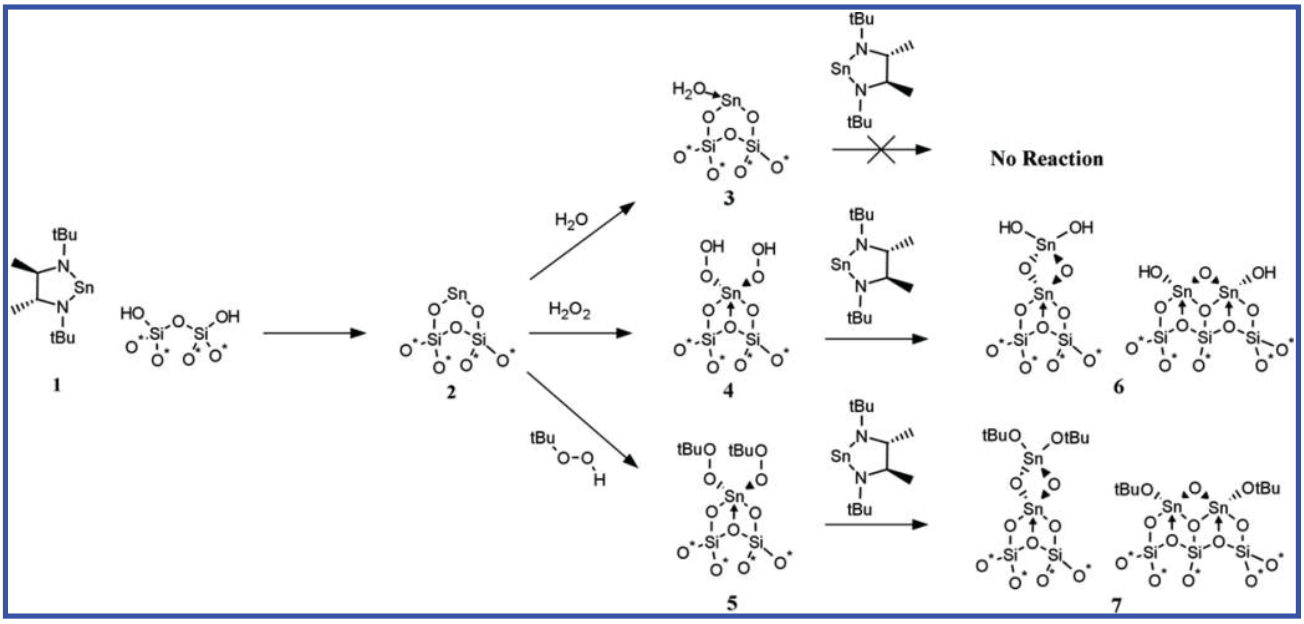

[a]Si−O* denotes a surface-bound species.

imately two first-shell scattering paths (both Sn−O bonds) and no higher order scatterers are present (Figure S1 in the Supporting Information). The lack of large clustering shown by these samples is in accord with Scotti and co-workers' research on tin-doped glass; a loading of less than 0.03 mol of Sn/mol of surface hydroxyls (3 mol %) produces a material with isolated SnO_2 sites.[20] From these data we can infer that the isolated Sn species remains in the 2+ oxidation state and is approximately two-coordinate and that **2** should have reactivity similar to a stannylene. Thus, we infer that **1** undergoes substitution through protonation with two neighboring surface silanol groups, generating free ligand in the process, similar to path A in Scheme 1. To the best of the authors' knowledge, this is the first observation of a surface-bound stannylene by X-ray absorption spectroscopy (XAS).

After establishing the isolated nature of **2**, that material was treated with water to produce a new orange material, **3**, as seen in Scheme 2. By XAFS, the coordination number of **3** increased from two to three as the bond length increased from 2.05(17) Å to 2.11(21) Å. It was determined through a difference fit that a full coordination of water is responsible for this lengthening of the average bond length. This result implies a picture where two Sn−OSi* bonds of 2.05 Å, one Sn−OH_2 bond of 2.15 Å, and the Sn lone pair fill the coordination sphere of the surface stannylene in a Lewis acid−base type reaction, shown in Scheme 2. This distance is in agreement with other sterically hindered stannylene−water Lewis acid−base compounds such as $[Sn(18\text{-crown-}6)(H_2O)][BF_4]_2{\cdot}2H_2O$, where the apical water is at a distance of 2.150(7) Å.[21] Since the reactivity with H_2O is a Lewis acid−base type, as shown as path B in Scheme 1, and not a protonation/deprotonation or oxidative addition type, the surface stannylene nature of **2** is further supported. One would also predict that **3** would be unreactive to further Sn(II) precursor and would not grow SnO by ALD. When **3** was exposed to a second molar equivalent of **1** (Scheme 2), there was no change in the XAS or Raman spectra, simply a darkening in the color of the material, further discussed below.

Exposure of **2** with strong oxidant sources, H_2O_2 and *t*BuOOH, gave two new white materials, **4** and **5**, respectively, as characterized by XAS. The judicious choice of oxidants provides a comparison of oxidants with similar strength, but with and without the presence of H_2O. As expected, both peroxides fully oxidized **2** to the 4+ state, as shown by a shift of 3.94 eV in the XANES spectrum (Table S1 of the Supporting Information). Additionally, the oxygen coordination number was found to be approximately six for **4** and **5**, which is in line with the Sn−O coordination of bulk SnO_2 and significantly greater than that of SnO. Additionally, the Sn−O bond length stays 2.05(17) Å, which is only marginally longer than bulk SnO_2 (2.042 Å) and much shorter than bulk SnO (2.231 Å). The structural similarities between **4** and **5** show that the presence of water does not affect the proposed growth mechanism, since care was taken to exclude water in the synthesis of **5**, and that **3** undergoes oxidative addition with peroxides. From Raman data we know that peroxide species exist on the surface of the high-surface-area silica for both **4**, 874 cm^{-1}, and **5**, 895 cm^{-1} (Figure 5 and Figures S7 and S8 in the Supporting Information). These values are in good agreement with the published values of the ν O−O mode,[22] but the resolution was not sufficient to distinguish between SiO-OR and SnO-OR species. From the XAFS data we also see an emergence of higher shell, Sn−O−Sn, scattering after peroxide treatment, as seen in Figures S3 and S4 in the Supporting Information. This is associated with Sn agglomeration; the amount of Sn−O−Sn in **4** was calculated to be 0.24(0.32) and 3.49(1.37) in **5**. While the uncertainty is substantial, the tin clustering is confirmed with Raman data as a peak emerging around 580 cm^{-1}.[20] The distance between Sn atoms is 3.23(0.01) Å for **4** and 3.30(0.14) Å for **5**, which is longer than the bulk value of 3.17(0.01) Å for SnO_2. From these data, we infer a mechanism similar to path C from

DOI: 10.1021/acs.organomet.5b01004
Organometallics 2016, 35, 1202−1208

Scheme 1, where oxidative addition occurs across the hydrogen−oxygen bond, generating surface-bound Sn(IV) species **4** and **5**, from Scheme 2, with at least one peroxide ligand.

With the nucleation and oxidation chemistry consisting of protonation followed by peroxide oxidation, we then added a second dose of tin precursor to the well-characterized Sn(II), **2** and **3**, and the Sn(IV), **4** and **5**, materials to elucidate the probable ALD growth mechanism. In the same fashion as the reaction with high surface silica, **2** and **3** react with a molar equivalent of **1** quickly in organic solvent, where the orange solution turns clear as the silica becomes deeper orange-brown, as seen in the higher molar loading (3.0%) in Figure 2c. These materials showed no change in the XAS or Raman spectra, consistent with the observation that bulk SnO is not grown from the tin precursor **1** and H_2O by ALD. Unlike the Sn(II) counterparts, the Sn(IV) materials, **4** and **5**, showed novel reactivity by XAS and Raman spectroscopy. The white material of **4** and **5** was added to an orange solution of **1**, and in less than 10 min, the solution became clear-colorless, while the material remained white. These new materials, **6** and **7**, showed only Sn(IV) by XANES, with no Sn(III) or Sn(II) apparent, but with an increase in the overall amount of Sn compared to **4** or **5** in the material. The XAFS spectra of **6** and **7** were essentially unchanged with respect to bond distances and coordination with respect to **4** and **5**. This means that the surface peroxide species observed in **4** and **5** are responsible for the complete oxidation of all newly introduced **1** to Sn(IV) and an excess of protons (from H_2O_2 or *t*BuOOH) is responsible for the removal of the diamido ligand. Disappearance of the ν O−O mode in the Raman spectrum of **6** and **7** further supports the peroxide-driven mechanism proposed (Figures S7 and S8, Supporting Information). Thus, it appears that a low-coordinate stannylene will react with surface peroxide species (Sn or Si) in a manner similar to path C in Scheme 1, faster than a proton transfer in path A. Unlike the initial nucleation by the protic ligand transfer mechanism, the steady-state growth mechanism likely involves the newly introduced stannylene insertion into a O−O bond of the peroxide, as shown on the left side of Scheme 2, and requires more peroxide to generate a reactive surface species, which allows for ALD-type growth. Thus, the mechanism for ALD growth of SnO_2 is as follows. First, **1** undergoes ligand exchange, by protonolysis, with surface hydroxyls to form a two-coordinate surface stannylene (**2**). Then a peroxide molecule oxidizes the surface stannylene, while excess H_2O_2 regenerates reactive surface peroxide species (**4**). Further vapor phase stannylene molecules react with the surface peroxide species, oxidatively inserting into the O−O bond and creating all Sn(IV) surface species (**6**). This insertion and oxidation occurs at a rate much faster than protonolysis, and ALD growth temperatures would limit the thermal lifetime of the surface-bound peroxide species.

CONCLUSIONS

In summary, we have mapped the likely deposition mechanism of a low-coordinate stannylene molecule, N^2,N^3-di-*tert*-butylbutane-2,3-diamidotin(II) (**1**), which successfully grows SnO_2 but not SnO by ALD with high-surface-area silica and three oxygen sources. X-ray absorption spectroscopy, diffuse reflectance infrared Fourier transform spectroscopy, and Raman spectroscopy show that the initial nucleation of **1** with the surface is nonoxidative. The surface stannylene contains isolated Sn(II) species that bind water without change in oxidation state. This new material, **3**, provided an example of a H_2O−stannylene Lewis acid−base complex. The surface stannylene reacts via well-defined oxidative addition with both aqueous and nonaqueous peroxide sources to yield surface Sn(IV). A "second dose" of **1** did not produce a reaction with the water-coordinated tin(II) stannylene, but surface peroxide groups bound to tin(IV) fully oxidized the second dose of tin precursor to 4+ without the observance of tin deposition in lower oxidation states. The thermal stability of the surface-bound tin(IV) peroxide is likely process-limiting for the growth of ALD SnO_2 with precursor **1**.

EXPERIMENTAL SECTION

General Considerations. All chemical manipulations were carried out using standard Schlenk techniques or in a glovebox (Vacuum Atmospheres) in a dry nitrogen atmosphere, with the exception of H_2O and H_2O_2 treatments. Pentane, diethyl ether, tetrahydrofuran (THF), toluene, benzene, and hexane were dried by argon-assisted movement over two columns (one neutral alumina column and one copper(II) oxide-Q5 column for pentane, toluene, benzene, and hexane and two neutral alumina for diethyl ether and THF), stored over 4 Å molecular sieves, and tested periodically with sodium benzophenone ketyl.[23] Synthesis of N^2,N^3-di-*tert*-butylbutane-2,3-diamidotin(II) (**1**) was performed according to literature procedures.[5] Hydrogen peroxide (30% in water from Sigma-Aldrich), *tert*-butyl hydroperoxide (5 M in decane from Sigma-Aldrich), and deionized water were deoxygenated with a moderate N_2 flow for a minimum of 15 min directly prior to use. High-surface-area silica (Sigma-Aldrich 250−500 μm, 35−60 mesh, 1.15 cm^3 pore volume, 150 Å pore size) was heated to 150 °C under reduced pressure (~25 mTorr) for over 5 h to remove chemisorbed water. All other reagents were obtained from commercial suppliers and used as received. IR data were taken in diffuse reflection mode on a Bruker FTIR model ALPHA-R spectrophotometer in DRIFT mode with a gold sample holder. Surface Raman measurements were taken with a red laser (785 nm) on a Renishaw spectrophotometer in a back-scattering configuration, using a Renishaw CCD camera and a 1200 nm slit. ^{1}H (300 MHz) NMR spectra were recorded on a Bruker 300 at ambient temperature and referenced to internal protio resonances.[24] NMR solvent was received from Cambridge Isotopes and dried over 4 Å molecular sieves for a minimum of 48 h prior to use.

Sn(II)@SiO_2 (2). Absorption of **1** on high-surface-area silica was performed by dissolving 77 mg (0.243 mmol) of **1** in 10 mL of pentane or hexane with a Teflon stir bar in a scintillation vial. Slowly, 1 g of high-surface-area silica was added, and the orange solution was allowed to stir for 1 h. The solution turned colorless within 10−30 min with a simultaneous color change of the silica to light orange. After this time, the solvent was removed under reduced pressure. This combination gave 2.9 wt % or 1.5 mol % of the desired product. Removal of free ligand was observed by ^{1}H NMR when a small amount of **2** was heated to 60 °C in 1 mL of C_6D_6.

Oxygen Source Treatment of 2. Reactions were carried out on **2** with different oxygen sources: H_2O (**3**), H_2O_2 (**4**), and ^{t}BuOOH (**5**). An indicative example is given below.

A 100 mL round-bottom flask with a Teflon stir bar and 15 mL of pentane was charged with 960 mg of **2**, then capped with a rubber stopper. Under nitrogen flow, 0.45 mL of *tert*-butyl hydroperoxide in decane (5.0 M, 2.25 mmol) was added, and the mixture was allowed to stir for 1 h. The solid turned colorless immediately. Volatile components were removed under reduced pressure, and **5** was further dried with 5 mL of toluene.

3 and **4** were synthesized in the same fashion with deoxygenated water as the solvent and without the toluene drying step.

Addition of a Second Diamido Sn (1) Treatment to 3, 4, and 5. Deposition of an additional molar equivalent of **1** was performed on all three oxygen source treatments to give two new materials: **6** from H_2O_2, and **7** from ^{t}BuOOH. A control was performed by addition of a

DOI: 10.1021/acs.organomet.5b01004
Organometallics 2016, 35, 1202−1208

second molar equivalent of **1** to **2**. A typical experiment is outlined below.

To a scintillation vial with a Teflon stir bar was added 12 mg (0.037 mmol) of **1**, then 5 mL of pentane. Then, 288 mg of **5** was added slowly, and the mixture was allowed to stir for 1 h. The orange solution turned colorless immediately for both **4** and **5**, while the solid stayed colorless. With **2** and **3** the solid darkened to an orange-red color as the solution became colorless.

X-ray Absorption Spectroscopy Experiments and Data Fitting Techniques. All X-ray experiments were carried out in Sector 10 at beamline-10-BM of The Materials Research Collaborative Access Team (MRCAT) at the Advanced Photon Source (APS). References and samples were pulverized in a mortar and pestle, in the amount of approximately 0.024 mmol of Sn, loaded, and pressed into sample holders in an airtight reactor, with a Kapton window, while under a nitrogen atmosphere in a glovebox. To ensure sufficient volume of sample, boron nitride was used for **1** and silica was used to supplement all other samples. X-ray absorption spectroscopy measurements were carried out around the Sn K edge (E_o = 29.2 keV) and collected in transmission mode using ionization gas chambers filled with >99% argon, <1% N_2. The energy of the X-ray photons was calibrated using a Sn metal foil, which was placed between the second and third gas chambers. Spectra were taken from −250 eV below to 800 eV above the absorption edge. XANES data were processed with the ATHENA program.

XAFS data curve fitting was performed in ATREMIS (version 0.8.014) and IFEFFIT software (version 1.2.11) by the FEFF program (0.8.061)[25] and by WinXAS (version 1.1). Scattering paths were calculated from SnO_2[26] and SnO[27] crystallographic information, as well as "quick first shell approximations" by FEFF for comparison. Data had the pre-edge and postedge backgrounds subtracted and then normalized to edge height. Background removal was accomplished through a seven-domain cubic-spline with a *k*-weight of two. To determine the phases and amplitudes, those data were Fourier transformed (FT) into *R* space, then back-Fourier transformed into *k* space. Amplitude reduction factors (S_0^2) were determined by using four scattering paths generated in IFEFFIT for SnO and SnO_2 while setting the coordination number of the scatters to the known crystal structures. These values were determined to be 0.97 for Sn(IV) species and 1.16 for the Sn(II) species (due to SnO_2 contamination) and thus set to 1. Coordination numbers of shells in unknown samples were then determined by setting S_0^2 and allowing the coordination number of the paths to vary independently. The disorder factor ($\Delta\sigma^2$), coordination number (N), and scattering distance (R) were then generated in this fashion from the experimental data (full tabulated data can be found in the Supporting Information).

WinXAS fits were performed as follows. After normalization, in the same fashion as before, and XANES analysis by inspection of the first derivative of the Sn *K* edge position, phase and amplitude references were extracted from the published crystal structure for the Sn−O path in SnO_2.[26] Once these parameters were experimentally determined, chemically realistic fits were attempted using a basic least-squares refinement. This was accomplished by allowing the program to find a best fit, then setting the $\Delta\sigma^2$ to provide realistic coordination numbers for the Sn−O path (full tabulated data can be found in the Supporting Information).

■ ASSOCIATED CONTENT

Supporting Information

The Supporting Information is available free of charge on the ACS Publications website at DOI: 10.1021/acs.organomet.5b01004.

Athena and WinXAS fit information table for compounds **2**−**7** with standards and XAFS figures for compounds **2**−**5**, Raman spectroscopy data for compounds **2**−**7** and controls, and DRIFTS data for compounds **3** and **5** (PDF)

■ AUTHOR INFORMATION

Corresponding Author

*E-mail (A. S. Hock): ahock@iit.edu.

Notes

The authors declare no competing financial interest.

■ ACKNOWLEDGMENTS

M.S.W. acknowledges support by the Department of Education GAANN Fellowship under Grant No. P200A090137. B.H. is thankful for a Starr Fieldhouse Fellowship. S.J.K. acknowledges the Department of Energy Contract No. DE-AC02-06CH11357. A.S.H. would like to thank the Department of Energy and the Illinois Institute of Technology for funding and startup support. MRCAT operations are supported by the Department of Energy and the MRCAT member institutions. This research used resources of the Advanced Photon Source, a U.S. Department of Energy (DOE) Office of Science User Facility operated for the DOE Office of Science by Argonne National Laboratory under Contract No. DE-AC02-06CH11357. The authors also thank Dr. Jeff Miller for assistance with XAS data analysis and Dr. Aditya Unni for donation of *tert*-butyl hydroperoxide.

■ REFERENCES

(1) (a) Tada, M.; Iwasawa, Y. *Coord. Chem. Rev.* **2007**, *251*, 2702−2716. (b) Chen, J.; Lim, B.; Lee, E. P.; Xia, Y. *Nano Today* **2009**, *4*, 81−95. (c) Bordiga, S.; Groppo, E.; Agostini, G.; van Bokhoven, J. A.; Lamberti, C. *Chem. Rev.* **2013**, *113*, 1736−1850.

(2) (a) Kingon, A.; Maria, J.; Streiffer, S. *Nature* **2000**, *406*, 1032−1038. (b) Markovich, G.; Collier, C. P.; Henrichs, S. E.; Remacle, F.; Levine, R. D.; Heath, J. R. *Acc. Chem. Res.* **1999**, *32*, 415−423.

(3) (a) Miikkulainen, V.; Leskelä, M.; Ritala, M.; Puurunen, R. L. *J. Appl. Phys.* **2013**, *113*, 021301. (b) Puurunen, R. L. *J. Appl. Phys.* **2005**, *97*, 121301. (c) Gordon, R. G. In *Atomic Layer Deposition for Semiconductors*; Hwang, C. S.; Yoo, C. Y., Eds.; Springer, 2014.

(4) Riha, S. C.; Racowski, J. M.; Lanci, M. P.; Klug, J. a; Hock, A. S.; Martinson, A. B. F. *Langmuir* **2013**, *29*, 3439−3445.

(5) Heo, J.; Hock, A. S.; Gordon, R. G. *Chem. Mater.* **2010**, *22*, 4964−4973.

(6) Kim, S. B.; Sinsermsuksakul, P.; Pike, R. D.; Gordon, R. G. *Chem. Mater.* **2014**, *26*, 3065−3073.

(7) Peng, Y.; Guo, J.-D.; Ellis, B. D.; Zhu, Z.; Fettinger, J. C.; Nagase, S.; Power, P. P. *J. Am. Chem. Soc.* **2009**, *131*, 16272−16282.

(8) Brown, Z. D.; Erickson, J. D.; Fettinger, J. C.; Power, P. P. *Organometallics* **2013**, *32*, 617−622.

(9) (a) Hahn, F. E.; Zabula, A. V.; Pape, T.; Hepp, A.; Tonner, R.; Haunschild, R.; Frenking, G. *Chem. - Eur. J.* **2008**, *14*, 10716−10721. (b) Akkari, A.; Byrne, J. J.; Saur, I.; Rima, G.; Gornitzka, H.; Barrau, J. *J. Organomet. Chem.* **2001**, *622*, 190−198. (c) Saur, I.; Rima, G.; Miqueu, K.; Gornitzka, H.; Barrau, J. *J. Organomet. Chem.* **2003**, *672*, 77−85. (d) Jana, A.; Roesky, H. W.; Schulzke, C.; Samuel, P. P. *Inorg. Chem.* **2010**, *49*, 3461−3464 for select examples.

(10) Gehrhus, B.; Hitchcock, P. B.; Lappert, M. F. *J. Chem. Soc. Dalt. Trans.* **2000**, 3094−3099.

(11) (a) Cotton, J. D.; Davidson, P. J.; Lappert, M. F.; Donaldson, J. D.; Silvet, J. *J. Chem. Soc., Dalton Trans.* **1976**, 2286. (b) Meltzer, A.; Inoue, S.; Präsang, C.; Driess, M. *J. Am. Chem. Soc.* **2010**, *132*, 3038−3046. (c) Saito, M.; Tokitoh, N.; Okazaki, R. *Organometallics* **1995**, *14*, 3620−3622. (d) Veith, M.; Müller, A. *J. Organomet. Chem.* **1988**, *342*, 295−301.

(12) (a) Cotton, J. D.; Davidson, P. J.; Lappert, M. F. *J. Chem. Soc., Dalton Trans.* **1976**, 2275. (b) Lappert, M. F.; Misra, M. C.; Onyszchuk, M.; Rowe, R. S.; Power, P. P.; Slade, M. J. *J. Organomet. Chem.* **1987**, *330*, 31−46. (c) Foley, S. R.; Yap, G. P. a.; Richeson, D. S. *J. Chem. Soc. Dalt. Trans.* **2000**, 1663−1668. (d) Zhou, D.; Reiche,

DOI: 10.1021/acs.organomet.5b01004
Organometallics 2016, 35, 1202−1208

C.; Nag, M.; Soderquist, J. A.; Gaspar, P. P. *Organometallics* **2009**, *28*, 2595−2608.
(13) (a) Harris, D. H.; Lappert, M. F. *J. Chem. Soc., Chem. Commun.* **1974**, 895. (b) Aubrecht, K. B.; Hillmyer, M. A.; Tolman, W. B. *Macromolecules* **2002**, *35*, 644−650. (c) Gans-Eichler, T.; Gudat, D.; Nieger, M. *Angew. Chem., Int. Ed.* **2002**, *41*, 1888.
(14) (a) Sinsermsuksakul, P.; Hartman, K.; Bok Kim, S.; Heo, J.; Sun, L.; Hejin Park, H.; Chakraborty, R.; Buonassisi, T.; Gordon, R. G. *Appl. Phys. Lett.* **2013**, *102*, 053901. (b) Sinsermsuksakul, P.; Chakraborty, R.; Kim, S. B.; Heald, S. M.; Buonassisi, T.; Gordon, R. G. *Chem. Mater.* **2012**, *24*, 4556−4562. (c) Sinsermsuksakul, P.; Heo, J.; Noh, W.; Hock, A. S.; Gordon, R. G. *Adv. Energy Mater.* **2011**, *1*, 1116−1125.
(15) Fix, R. M.; Gordon, R. G.; Hoffman, D. M. *J. Am. Chem. Soc.* **1990**, *112*, 7833−7835.
(16) Foley, P.; Zeldin, M. *Inorg. Chem.* **1975**, *14*, 2264−2267.
(17) Neumann, W. P. *Chem. Rev.* **1991**, *91*, 311−334.
(18) Morrow, B. A.; McFarlan, A. J. *J. Non-Cryst. Solids* **1990**, *120*, 61−71.
(19) Gardiner, M. G.; Raston, C. L. *Inorg. Chem.* **1995**, *34*, 4206−4212.
(20) Chiodini, N.; Morazzoni, F.; Paleari, A.; Scotti, R.; Spinolo, G. *J. Mater. Chem.* **1999**, *9*, 2653−2658.
(21) Beattie, C.; Farina, P.; Levason, W.; Reid, G. *Dalton Trans.* **2013**, *42*, 15183−15190.
(22) Venkateswaran, S. *Nature* **1931**, *127*, 406−406.
(23) Pangborn, A. B.; Giardello, M. A.; Grubbs, R. H.; Rosen, R. K.; Timmers, F. J. *Organometallics* **1996**, *15*, 1518−1520.
(24) Gottlieb, H. E.; Kotlyar, V.; Nudelman, A. *J. Org. Chem.* **1997**, *62*, 7512−7515.
(25) (a) Newville, M. *J. Synchrotron Radiat.* **2001**, *8*, 322−324. (b) Ravel, B.; Newville, M. *J. Synchrotron Radiat.* **2005**, *12*, 537−41. (c) Ravel, B. *J. Synchrotron Radiat.* **2001**, *8*, 314−316.
(26) Yamanaka, T.; Kurashima, R.; Mimaki, J. *Z. Kristallogr. - Cryst. Mater.* **2000**, *215*, 424.
(27) Batzill, M.; Diebold, U. *Prog. Surf. Sci.* **2005**, *79*, 47−154.

DOI: 10.1021/acs.organomet.5b01004
Organometallics 2016, 35, 1202−1208